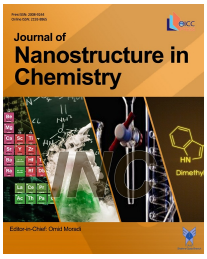

Volume 15, Issue 1, 152502 (1-10)

JNSC**15** (2025) -152502 1/10

Journal of Nanostructure in Chemistry (JNSC)

https://doi.org/10.57647/jnsc.2025.1501.02

Ti_3C_2 MXene-Enhanced Electrochemical Biosensors for Prostate-Specific Antigen (PSA) Detection in Prostate Cancer

Lyu Jia[1], Zhangming Lei[2], Najmeh Zare[3,*], Tao Wu[4], Masoumeh Ghalkhani[5], Lijun Wan[2,*], Yi Xu[3,*]

[1]*Urology & Nephrology Center, Department of Urology, Zhejiang Provincial People's Hospital (Affiliated People's Hospital, Hangzhou Medical College), Shangtang Road 158, Hangzhou, Zhejiang, China.*
[2]*Department of Urology, The Quzhou Affiliated Hospital of Wenzhou Medical University, Quzhou People's Hospital, Quzhou, Zhejiang 324000, PR China.*
[3]*Department of Urology, Department of Science & Technology, BioSensorMed Research Group, The Quzhou Affiliated Hospital of Wenzhou Medical University, Quzhou People's Hospital, Quzhou, Zhejiang 324000, PR China.*
[4]*School of Resources and Environment, University of Electronic Science and Technology of China, 611731, Xiyuan Ave, Chengdu, China.*
[5]*Electrochemical Sensors Research Laboratory, Department of Chemistry, Faculty of Science, Shahid Rajaee Teacher Training University, Lavizan, Tehran, Iran.*

[*]**Corresponding authors:** najmeh.zare.1997@gmail.com, qywanlijun@wmu.edu.cn, yixu@wmu.edu.cn

Original Research

Received:
1 January 2025
Revised:
15 February 2025
Accepted:
17 February 2025
Published online:
28 February 2025

Abstract:

Prostate cancer ranks among the most prevalent malignancies affecting the male population globally, where its elevated mortality rate is frequently ascribed to the tardiness of diagnosis. Traditional diagnostic techniques, such as digital rectal examinations, are often associated with discomfort and may lead to postponements, as they conventionally necessitate further validation via biopsies and Gleason grading. Therefore, many efforts have been made to design new and widely used methods. This study investigates the design and implementation of electrochemical biosensors enhanced with Ti_3C_2 MXene for the accurate and sensitive quantification of prostate-specific antigen (PSA), an essential diagnostic marker indicative of prostate cancer. This biosensor was developed by modifying a carbon-based screen-printed electrode (SPCE) utilizing nanoparticles of gold (Au-NPs) and a Ti_3C_2 MXene layer, integrated with a Cd^{2+}-binding aptamer (SPCE/Ti_3C_2MXene/Au-NPs/Cd^{2+}-aptamer). The biosensor's specificity for PSA was ensured through the immobilization of PSA-recognition aptamers on the Ti_3C_2 MXene/Au-NPs-enhanced SPCE surface. The Ti_3C_2 MXene layer was synthesized and examined with different characterization tools, like transmission electron microscopy (TEM), X-ray photoelectron spectroscopy (XPS), scanning electron microscopy (SEM), energy-dispersive X-ray spectroscopy (EDS), fourier-transform infrared spectroscopy (FTIR), and X-Ray diffraction analysis (XRD), serving as a conductive support that helped integrate of the biological recognition element. The electrochemical signals generated from the Cd^{2+} complexed with the aptamer at the sensor interface allowed for quantitative assessment of PSA levels, revealing a detection range from 1.0 to 300 pg/mL and an impressive detection threshold as low as 8.0 fg/mL. This innovative biosensor exhibited excellent selectivity in detecting PSA among other biomarkers, highlighting its potential for clinical applications in prostate cancer diagnostics.

Keywords: Aptamer; Biosensor; Hybrid composite; Prostate-specific antigen; Ti_3C_2 MXene

Cite this article: Jia, L., Lei, Zh., Zare, N., Wu, T., Ghalkhani, M., Wan, L., Xu, Y. Ti_3C_2 MXene-Enhanced Electrochemical Biosensors for Prostate-Specific Antigen (PSA) Detection in Prostate Cancer. *J Nanostruct Chem* **15**(1), 1-10 (2025).

1. Introduction

Biomarkers are used to track and obtain vital information about physiological processes, disease status and progression, or response to therapeutic interventions [1–4]. Biomarkers fall into several main groups: diagnostic biomarkers used to identify diseases, those that monitor disease progression, and those that predict a patient's response to specific treatments. Biomarkers that can produce a large response-to-noise ratio and good selectivity are more effective [5–7]. They are also essential in public health for monitoring disease outbreaks and evaluating intervention effectiveness [8]. The growing emphasis on health span research underscores the importance of collaboration between fundamental biologists and clinical researchers, as these partnerships can enhance treatment outcomes and address challenges in biomarker discovery and validation [9, 10].

Ranking among the most common male malignancies, prostate cancer (PC) stands as the second most common cause of cancer-related mortality for those aged 45 and above, surpassed only by lung cancer [11]. The diagnosis of PC is particularly challenging because it progresses slowly and often shows no early symptoms, leading to diagnoses at more advanced stages when curative treatments may no longer be viable [12, 13]. The prompt identification of cancer is essential for successful treatment and greatly improves patients' quality of life. One effective strategy involves identifying cancer biomarkers in serum or blood, which serve as vital diagnostic tools in the medical field. This technique allows for not only the timely recognition of cancer but also offers valuable insights into the likely progression of the disease and the effectiveness of treatment options. By monitoring these biomarkers, clinicians can tailor therapeutic approaches to individual patients, enhancing their overall care and outcomes [14]. PSA, a protein crucial for diagnosing prostate cancer, can also increase in noncancerous conditions like trauma, infection, inflammation, and non-malignant prostate growth [15]. While PSA is widely used to assess various prostate-related disorders, established diagnostic tools such as enzyme-linked immunoassay-based methods and polymerase chain reaction (PCR), and radioimmunoassay present challenges, including high costs, complex equipment, and inadequate sensitivity. These limitations highlight the need for innovative and efficient PSA detection methods to improve early diagnosis and treatment options for patients [16, 17]. Simplifying analytical methodologies might unexpectedly enhance diagnostic accuracy and therapeutic outcomes.

The nanotechnology revolution in materials engineering has fundamentally reshaped industrial implementation paradigms [18–21]. Utilized in medicine, electronics, agriculture, and construction, these materials stand out due to their unique properties [22–26]. MXenes represent a class of 2D materials comprising transition metal carbides, nitrides, and carbonitrides, characterized by the universal metal carbides, nitrides, and carbonitrides, charactrized by the universal chemical structure $M_{n+1}X_nT_x$ [27]. In this formula, M represents a d-block element, X stands for carbon or nitrogen atoms, while T corresponds to terminal moieties including –OH or –F groups. Emerging from a decade of research on 2D materials, MXenes have gained recognition as "wonder materials" since their discovery in 2011 [28], primarily due to their impressive properties [29]. They exhibit remarkable electrical conductivity, expansive surface area, and impressive electrochemical performance [30]. Such multifunctionality allows broad implementation across technologies, including but not limited to catalysis, energy storage, and saltwater treatment. The unique combination of their 2D structure and rich surface chemistry allows for rapid ion transport and enhances their functionality in various systems, making them a pivotal material in modern technology [31, 32]. MXenes have found applications across diverse fields, including soft electronics, sensors, and biomedical devices [33, 34]. Their ability to form hydrogels enhances their stability and opens new avenues for flexible energy storage and human-machine interfaces [35, 36]. These MXene-based hydrogels boost the materials' inherent properties, leading to improved performance in applications such as energy harvesting and catalysis. Importantly, the integration of MXenes into sensor technologies has shown promise, particularly in the development of biosensors [37]. The tunable surface functionalities of MXenes can be tailored for specific biological interactions, enabling sensitive detection of biomolecules. Among the MXenes, Ti_3C_2 stands out due to its remarkable electrochemical properties, making it particularly effective for electrochemical sensors and biosensors [38, 39]. Ti_3C_2 exhibits high conductivity and a large surface area, promoting rapid electron transfer and enhancing the sensitivity of electrochemical reactions. These characteristics make Ti_3C_2 an excellent candidate for detecting various biomolecules, including glucose, DNA, and proteins. The surface functional groups on Ti_3C_2 can be modified to improve selectivity for specific targets, further increasing the performance of biosensors [40, 41]. Ti_3C_2 MXene holds significant potential in advancing the field of electrochemical sensing, providing highly sensitive and specific detection capabilities crucial for medical diagnostics and environmental monitoring [42, 43]. These attributes not only enable the development of portable, low-cost biosensing devices but also address key challenges in early disease detection and real-time environmental monitoring. By seamlessly integrating nanomaterial innovation with practical sensing requirements, Ti_3C_2 MXene holds immense potential to transform point-of-care diagnostics and sustainable monitoring technologies on a global scale [29].

Aptamer electrochemical biosensors for prostate cancer diagnosis face limitations, such as sensitivity to environmental conditions and potential instability of aptamers over time. Additionally, challenges include the need for precise calibration and the complexity of sample matrices, which can interfere with accurate detection. This research focused on creating a label-free electrochemical sensing device based on aptamers, utilizing Ti_3C_2 MXene nanosheets integrated with Au NPs to boost the detection performance of the biomarker PSA. Cd^{2+}-loaded, thiolated PSA aptamers were anchored to the SPCE surface to create the recognation interface. The resulting biosensor provides a non-invasive solution for PSA quantification, supporting prostate cancer management.

To quantify the aptamer-complexed cadmium ion serving as an electrochemical reporter, the Anodic Stripping Square Wave Voltammetry (ASSWV) was employed, providing a highly sensitive measurement technique. Signal variations were detected upon the liberation of Cd^{2+} ions from the Ti_3C_2 MXene/Au NPs surface due to the interaction between PSA and the aptamer. This innovative design not only enhances sensitivity but also enables real-time tracking of PSA levels, playing a critical role in timely intervention in prostate cancer treatment.

2. Experimental procedures

2.1 Chemical components and reactants

The materials employed here were purchased from famous suppliers to ensure compliance with analytical standards without the need for additional purification. Titanium Aluminum Carbide (Ti_3AlC_2) was acquired from Laizhou Kai Kai Ceramic Materials Co., Ltd. (Shandong, China), specializing in high-quality ceramic materials. Additionally, Tris(hydroxymethyl)aminomethane (Tris), 6-Mercaptohexanol (MCH), HF 48%, Tris(2-carboxyethyl) phosphine hydrochloride (TCEP), and Cadmium Nitrate Tetrahydrate were sourced from Adamas reagents (Shanghai Titan Scientific Co., Ltd., China). Finally, the thiolated-DNA aptamer having the sequence of 5′-SH/-TTTTTA ATT AAA GCT CGC CAT CAA ATA GCT TT-3′ was supplied by Sangon Biotech (Shanghai, China).

2.2 Instruments

Electrochemical signals for monitoring of PSA using SPCE/Ti_3C_2 MXene/Au-NPs were recorded by Metrohm DropSensb (μState- I 400). FT-IR characterization of Ti_3C_2-MXene was performed by FTIR-850. Crystalline structure of Ti_3C_2 MXene was analyzed by X-ray diffraction (XRD) using a BRUKER D8 ADVANCE diffractometer (Germany), while surface chemistry was examined through X-ray photoelectron spectroscopy (XPS) with a Thermo Scientific K-Alpha system (ThermoFisher, USA). Field emission scanning electron microscope (FESEM, Apreo 2S, ThermoScientific, US) and Transmission Electron Microscope (TEM, Tecnai G2 F20, FEI, USA) were employed for morphological and structure analysis of Ti_3C_2 MXene.

2.3 Ti_3C_2-MXene synthesis

The synthesis of MXene refers to previous reports [44]. First, 1.0 g of Ti_3AlC_2 powder was placed into a polytetrafluoroethylene container. The process was followed by the addition of 15 mL of 48% HF to the container, with stirring at ambient temperature for duration of 48 hours. After etching, the mixture was cleaned multiple times with deionized water until a pH of approximately 6 was reached. The black end product was subjected to vacuum drying at 80 °C for a period of 12 hours.

2.4 Biosensor preparation

The electrochemical assessment was executed in a buffered solution (10 mM Tris-HCl), maintained at pH 7.5. A 5.0 μL aliquot of 0.5 mg/mL Ti_3C_2-MXene suspension was drop-casted onto the surface of a SPCE. The electrode was left to evaporate the solvent and dried under infrared light. The gold deposition on the SPCE/Ti_3C_2-MXene was performed in 0.01 M $HAuCl_4$ electrolyte containing KCl (0.1 M) at −0.3 V for duration of 1 min, followed by air-drying. Subsequently, the Cd^{2+}-recognition aptamers were anchored to the Ti_3C_2-MXene/Au NPs surface via 12 h cold incubation (4 °C). After removing unbound materials with Tris-HCl rinsing, 1.0 mM MCH was applied for 1 h to complete surface functionalization. The aptasensor was rinsed again to remove excess MCH and then exposed to a PSA solution prior to electrochemical measurements using ASSWV, as detailed in Scheme 1.

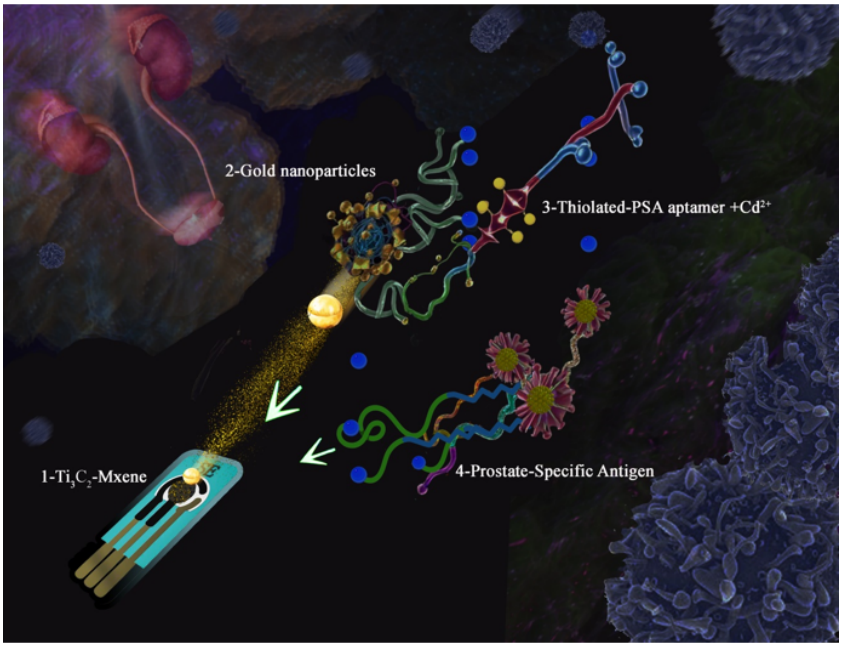

Scheme 1. Design strategy and assembly process of the PSA-specific aptasensor.

3. Results and discussions

3.1 Characterizing nanomaterials

FT-IR spectra and XRD patterns of MXene are illustrated in Fig. 1. In Fig. 1 (a), the band at 3134 cm^{-1} was derived from the stretching vibration of the -OH groups present on the material surface [45]. The characteristic peaks around 1629 cm^{-1} and 609 cm^{-1} were ascribed to the C=O and Ti-O moieties on the surface of the material [46]. The weak characteristic band at 1043 cm^{-1} may be attributed to the vibration of the C-F group according to the reported literature [47]. It can be seen from Fig. 1 (b) that Ti_3AlC_2 has several typical characteristic XRD peaks, such as (002) and (104). The peak (104) disappeared after HF etching, indicating that the Al layer was etched out. The peak (002) moved to 8.9°, and the intensity and width of the diffraction peak became larger. This phenomenon indicates that the MXene surface will form negative moieties (-OH, -OOH, and -F) after Al is etched. The electrostatic interaction between these functional groups causes the layer spacing to increase, which causes the (002) diffraction peak to shift to a smaller angle.

The morphology and microstructure of MXene were evaluated utilizing SEM and TEM techniques, and the specific outputs are shown in Fig. 2. An obvious two-dimensional multi-layer stack structure was observed for MXene after etching the Al layer with HF (Fig. 2 (a-c)), indicating that MXene has been successfully synthesized [48]. The EDS characterization outputs in Fig. 2 (d) show that the prepared MXene composite material consists of four elements, C, O, F, and Ti, indicating, from another perspective, the successful preparation of MXene material. TEM shows that MXene is a multi-layer structure stacked on each other (Fig. 2 (e-f)). The high-resolution TEM shown in Fig. 2 (g) shows the lattice plane spacing of the MXene material.

The chemical composition and surface valence of MXene were further analyzed by XPS (Fig. 3). According to Fig. 3 (a), the four elements of C, O, Ti, and F are main constituents of MXene, consistent with those of the EDS experiment (Fig. 2 (d)). In the C 1s spectrum depicted in Fig. 3 (b), the four peaks at 286.2, 284.8, 282.8, and 281.9 eV originate from C-O, C-C, C-Ti, and C-Ti-O, in sequence [49]. The O 1s response was divided into three peaks of s at 532.5, 531.8, and 529.6 eV, which can be assigned to C-O, C-OH, and TiO_2 [50]. Deconvolution of the Ti 2p spectrum revealed five distinct components at binding energies of 462.2 eV (Ti^{2+} $2p_{1/2}$), 461.0 eV (Ti^{3+} $2p_{1/2}$), 458.4 eV (Ti^{4+} $2p_{3/2}$), 455.8 eV (Ti^{2+} $2p_{3/2}$), and 454.9 eV (Ti^{3+} $2p_{3/2}$) [48, 50].

3.2 Electrochemical analysis

3.2.1 Biosensor modification studies

The biosensor's performance and surface modifications were systematically evaluated using cyclic voltammetry (CV) alongside electrochemical characterization, with the $[Fe(CN)_6]^{3-/4-}$ redox probe serving as a standard electrochemical indicator. The CV evaluation for the bare SPCE (Fig. 4 (curve a)) showed a quasi-reversible behavior with a wide peak-to-peak separation ($\Delta E = 434$ mV) and an oxidation current of 66.3 µA, while it revealed notable current enhancements when modified with Ti_3C_2-MXene (curve b) ($I_{pa} = 96.5$ µA), without any catalytic effect since the peak potential stayed almost unchanged. A greater improvement was observed with the addition of Au NPs (curve e), bringing a reversible behavior for the $[Fe(CN)_6]^{3-/4-}$ redox reaction ($I = 166.4$ µA; $\Delta E = 88$ mV).

These findings underscore the significant electrochemical impact of both Ti_3C_2-MXene and Au NPs, validating the effectiveness of the modification process. After integrating the Cd^{2+}-aptamer into the Ti_3C_2-MXene/Au NPs system, a reduction in anodic current was observed (curve d), indicating that an insulating thin layer formed on the SPCE/Ti_3C_2-MXene/Au NPs surface ($I = 150.1$ µA; $\Delta E = 99$ mV). The introduction of the PSA protein caused an additional decline in anodic response for the SPCE/Ti_3C_2-MXene/Au NPs/Cd^{2+}-aptamer configuration (curve c), which may stem from the inherent low conductivity of the immobilized protein structure (I26.2 µA; $\Delta E = 330$ mV).

3.2.2 Optimization of critical biosensor parameters

To boost the aptasensor's sensing performance, the influence of varying Cd^{2+} concentration and incubation times with the PSA solution was evaluated (Fig. 5 (A) and (B)). The chart in Fig. 5 (A) indicates that the concentration increment of Cd^{2+} ions ($0.5 - 5$ mM) significantly improved the ASSWV current, demonstrating that higher concentrations improved Cd^{2+} capture efficiency by the immobilized

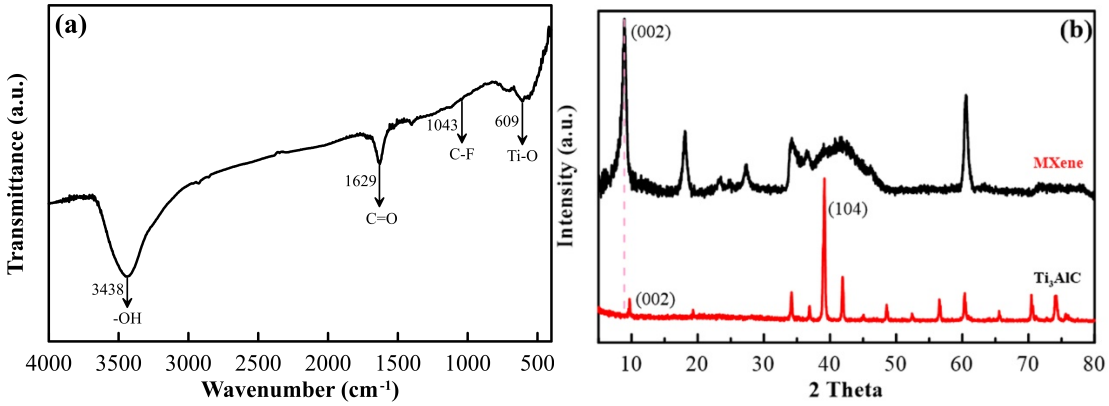

Figure 1. (a) FT-IR pattern of MXene and (b) XRD spectra of Ti_3AlC and MXene.

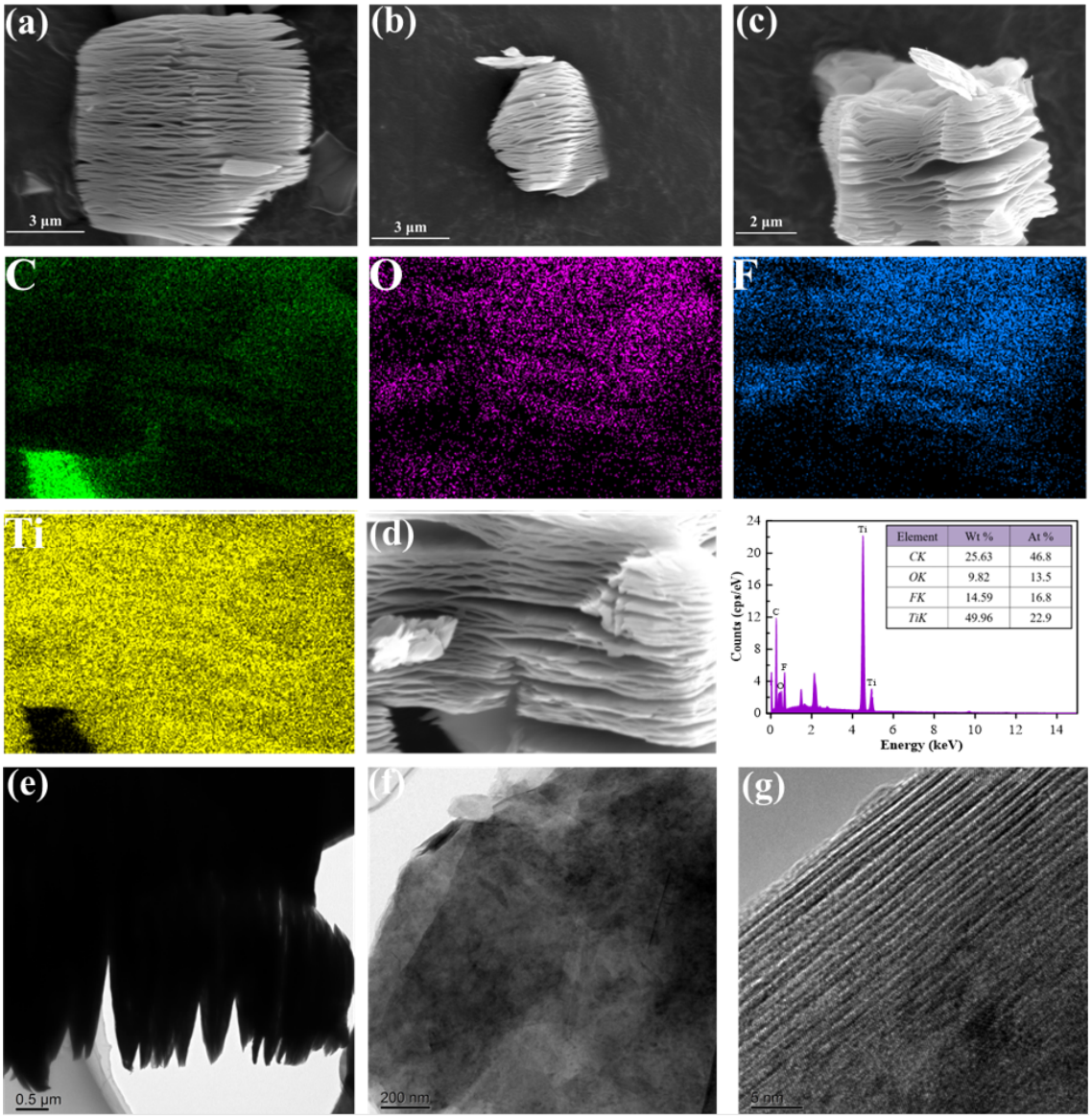

Figure 2. SEM results of MXene (a-c), Elemental mapping and EDS spectrum of MXene (d), and TEM image of Multi-layer MXene (e-g).

aptamer, subsequently, which is essential for the aptasensor's functionality. The biosensor response plateaued at Cd^{2+} concentrations above $5-6$ mM, indicating complete saturation of aptamer binding sites, where additional analyte failed to increase signal output. In terms of incubation time, Fig.Fig. 5 (B) reveals that extending the exposure to PSA to 90 minutes led to a significant attenuation of the ASSWV current response for Cd^{2+} detection, as PSA effectively displaced Cd^{2+} from the biosensor structure, eliminating it from the functionalized biosensor surface. After 90 minutes, the voltammetric response for Cd^{2+} attained stability, demonstrating equilibrium conditions in the aptamer-analyte binding system. Additionally, Fig. 5 (C) examines the impact of various buffer solutions on biosensor activity, highlighting that Tris-HCl outperformed PBS and Britton-Robinson, leading to its selection for further experimental steps. This comprehensive analysis emphasizes the key factors influencing the aptasensor's efficiency and lays the groundwork for future optimization efforts.

3.3 Assessment of the biosensor's analytical performance

It was focused on evaluating the effectiveness of the SPCE/Ti_3C_2-MXene/Au NPs/Cd^{2+}-aptamer in monitoring the prostate tumor-selective biomarker, utilizing ASSWV. The interaction between the aptamer and PSA was assessed by conducting ASSWV measurements in both the absence and presence of PSA at concentrations of 50.0 and 120 pg/mL, as depicted in Fig. 5 (D). A significant decrement of the ASSWV peak current was observed following the PSA introduction (curves b and c). This signal reduction reflects PSA-specific aptamer binding at the modified electrode surface, causing Cd^{2+} displacement that diminishes the ASSWV response. Control experiments with non-specific proteins showed $< 5\%$ signal variation. These results demonstrate the biosensor's specific PSA detection capability, with signal attenuation (ΔI) exhibiting linear correlation to PSA concentration ($1-300$ pg/mL, $R^2 = 0.9949$). The SPCE/Ti_3C_2-MXene/Au NPs/Cd^{2+}-aptamer platform achieved clinically relevant sensitivity

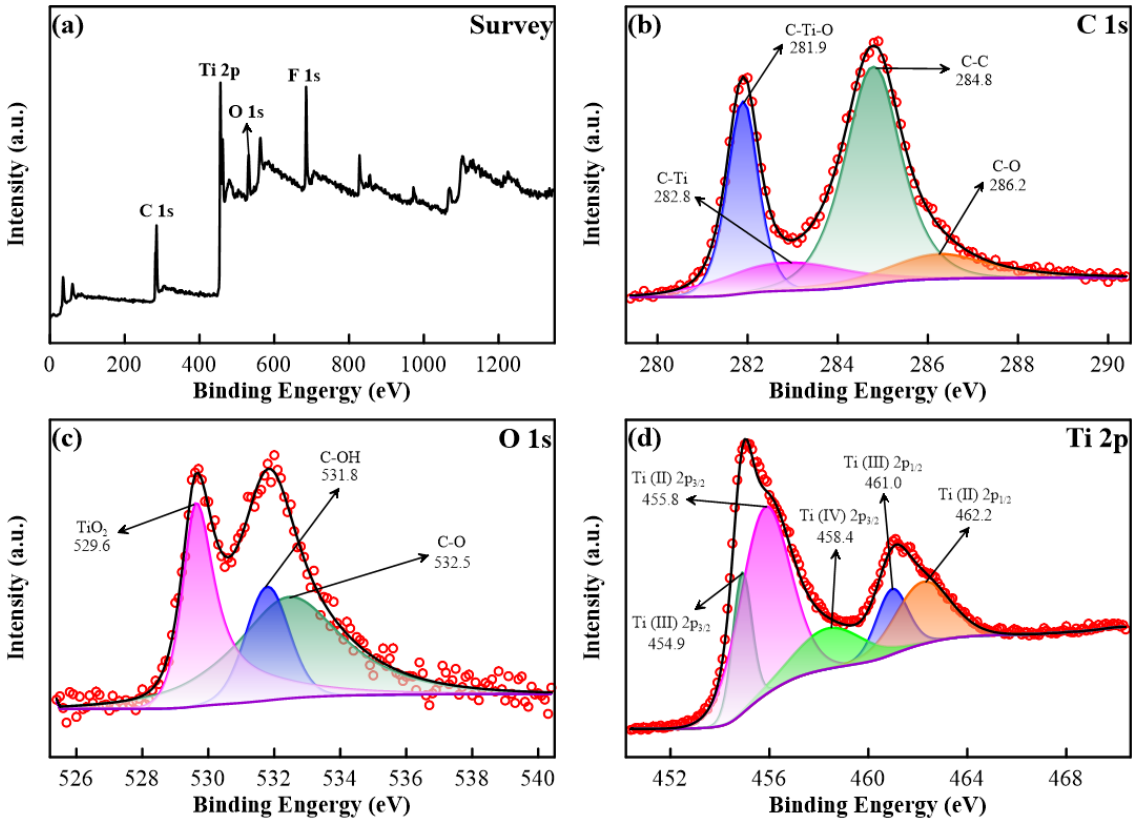

Figure 3. XPS characterization of MXene. (a) Complete survey spectrum, (b) C 1s, (c) O 1s, and (d) Ti 2p high-resolution regions.

for prostate cancer monitoring, as evidenced by the calibration curve $\Delta I = 0.101C + 1.4295$ (Fig. 6).

Significantly, the sensor achieved an impressive detection limit (LOD) of 8.0 fg/mL, outperforming earlier reported sensors (Table 1). Unlike conventional methods requiring complex sample preparation, our design enables rapid detection with minimal pretreatment. These advancements position our biosensor as a transformative tool for non-invasive prostate cancer monitoring, addressing critical limitations in sensitivity, specificity, and clinical practicality of current diagnostic approaches.

The SPCE/Ti_3C_2-MXene/Au NPs/Cd^{2+}-aptamer selectivity for detecting PSA was evaluated in comparison to other prostate biomarkers, including PSMA, PAP, and FASN. As illustrated in Fig. 7 (A), the biosensor demonstrated a satisfactory level of selectivity for PSA.

In terms of stability, the biosensor's response to a concentration of 80 pg/mL PSA was tracked over several weeks. As

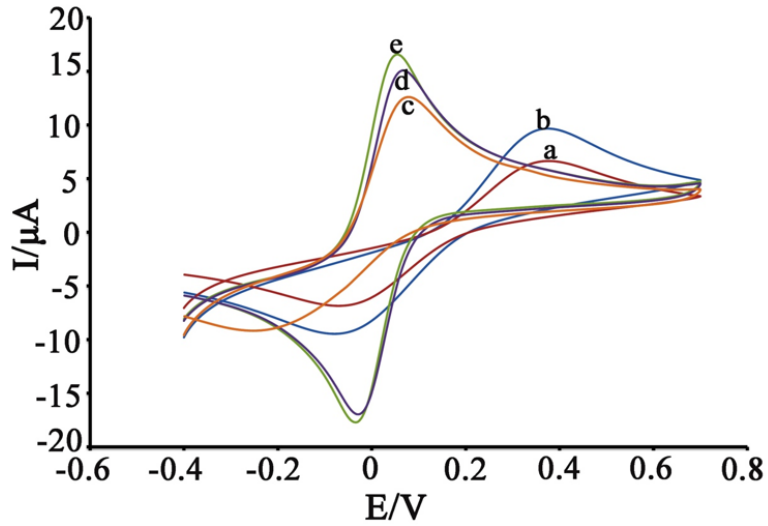

Figure 4. CVs for the following electrode configurations: (a) The unmodified SPCE, (b) SPCE/Ti_3C_2 MXene, (c) SPCE/Ti_3C_2 MXene/Au NPs/Cd^{2+}-aptamer-PSA, (d) SPCE/Ti_3C_2 MXene/Au NPs/Cd^{2+}-aptamer, and (e) SPCE/Ti_3C_2 MXene/Au NPs employing a 1.0 mM $[Fe(CN)_6]^{3-/4-}$ solution as redox mediator.

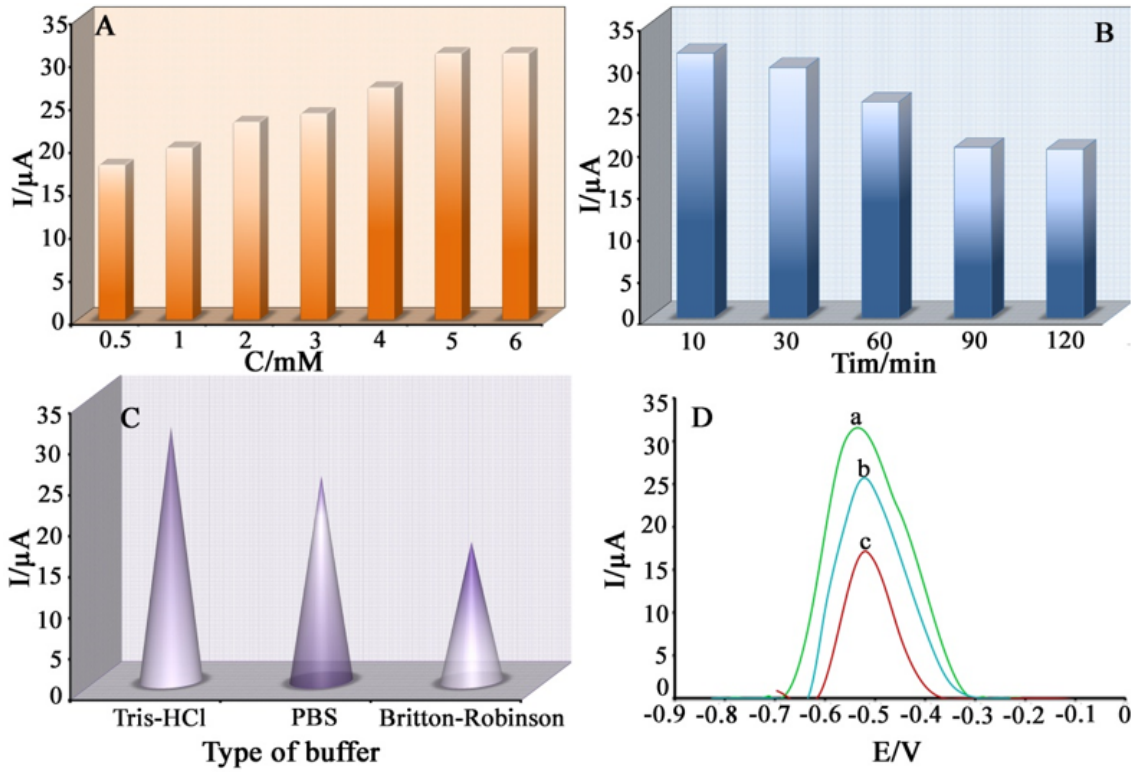

Figure 5. (A) Cd^{2+} concentration optimization. (B) Incubation time optimization with PSA. (C) Buffer solution effects on the detection signal. (D) Anodic stripping voltammetry revealing biosensor response without (a) and with PSA at (b) 50 pg/mL and (c) 120 pg/mL.

illustrated in Fig. 7 (B), it maintained strong performance during the initial three weeks. A decline in detection capability was observed beyond this time frame. These findings indicate that the biosensor can effectively detect PSA for approximately 21 days, after which its accuracy in quantification begins to diminish. The accuracy of the developed electrochemical aptasensing platform for the analysis of real samples was checked by monitoring of spiked PSA in serum samples, and results showed a recovery range of 96.8% − 103.5%, which confirms SPCE/Ti_3C_2-MXene/Au NPs/Cd^{2+}-aptamer ability in monitoring of PSA. The next generation of MXene-based biosensors will likely emerge from current research efforts focusing on material optimization and device architecture, potentially achieving the reliability and performance required for mass production and real-world deployment in healthcare and field applications.

4. Conclusion

This article introduces an innovative biosensor designed for the precise detection and monitoring of the PSA prostate cancer biomarker through a sophisticated layered approach using a designed Ti_3C_2-MXene/Au NPs/Cd^{2+}-aptamer

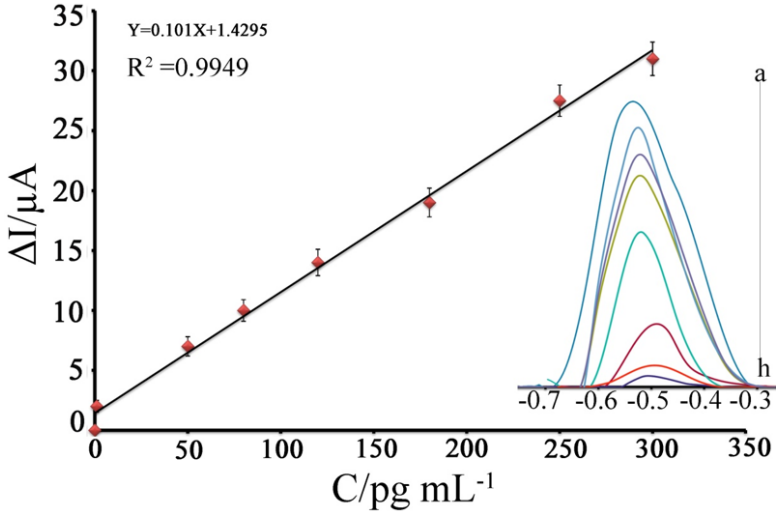

Figure 6. Quantitative performance of the PSA biosensor. The inset displays ASSWV signals for PSA solutions ranging from 0.0 to 300 pg/mL (a-h) at SPCE/Ti_3C_2-MXene/Au NPs/Cd^{2+}-aptamer (n = 3).

Table 1. Performance evaluation of the SPCE/Ti_3C_2-MXene/Au NPs/Cd^{2+}-aptamer for the PSA analysis.

Electrode	Modifier	LDR	LOD	Ref.
GCE	Reduced graphene oxide decorated with gold nanoparticles	25 – 36 ng/mL	2 pg/mL	[51]
GCE	Hemin-functionalized graphene-conjugated palladium nanoparticles	0.025 – 25 ng/mL	8.0 ng/mL	[52]
SPCE	Molybdenum disulfide quantum dots	0.01 pg/mL to 200 ng/mL	0.01 pg/mL	[53]
96-well microtiter plate	AuNP + peptide	80 pg – 7 ng/mL	30 pg/mL	[54]
SPCE	Ti_3C_2-MXene/Au NPs/Cd^{2+}-aptamer	1.0 – 300 pg/mL	8.0 fg/mL	Current study

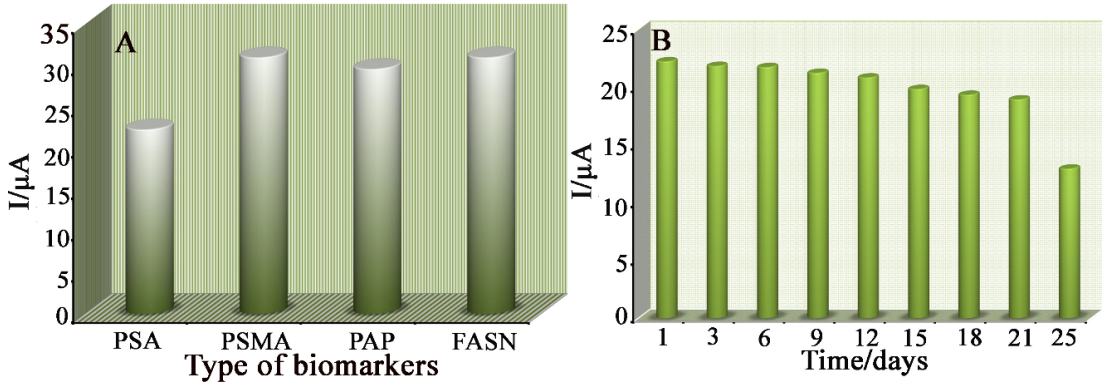

Figure 7. (A) Evaluation of the PSA aptasensor's selectivity. (B) Stability of the electrochemical aptasensor for PSA detection over a 25-day period.

layer as the SPCE modifier. The biosensor primarily functions to identify PSA's presence, employing Cd^{2+} as a redox-active reporter for quantitative detection. The biosensor demonstrates a wide linear detection range (1.0 – 300 pg/mL) with an impressive LOD of 8.0 fg/mL (S/N = 3), surpassing conventional ELISA methods (typical LOD: ∼ 10 pg/mL). Notably, the biosensor exhibits exceptional selectivity for PSA, with negligible interference from other potential confounders such as PSMA, PAP, and FASN. The detection limit and appropriate linear range with excellent selectivity are the most important advantages of the proposed biosensor compared to other works. This advancement suggests that the biosensor could significantly reduce the need for invasive procedures in prostate cancer treatment. Future studies exploring MXene customization and system integration could further improve both specificity and durability, facilitating their commercialization for medical diagnostics and on-site monitoring applications.

Authors Contribution

Conceptualization, A. A.; Methodology, M. B, H. M and E. F; formal analysis, E. F; investigation, A. A.; resources, M. B and A. A.; Writing original draft preparation, A. A, N. S and H. M; writing review and editing, M. B.; supervision, M. B; project administration, A. A and M. B; funding acquisition, A. A. All authors have read and agreed to the published version of the manuscript.

Availability of data and materials

The data that support the findings of this study are available from the corresponding author, upon reasonable request.

Conflict of interests

The authors declare that they have no known competing financial interests or personal relationships that could have appeared to influence the work reported in this paper.

References

[1] Y. Jia, S. Chen, Q. Wang, and J. Li. "Recent progress in biosensor regeneration techniques ". *Nanoscale*, **16**(6):2834–2846, 2024.

[2] N. Zare, H. Karimi-Maleh, Z. Zhang, L. Fu, J. Rouhi, N. Zhong, Y. Wen, and M. Ghalkhani. "Enhancing cancer biomarker identification: precise monitoring of MUC1 using V2C/Au nanocomposite-amplified electrochemical biosensor ". *Carbon Lett.*, 2025.

[3] Q. Jia and H. Cao. "Innovative CuO worm-shaped@ $BiVO_4$ photoelectrochemical biosensor for enhanced glucose detection in athletes' biological samples". *Alex. Eng. J.*, **124**:12–23, 2025.

[4] D. Bhatia, S. Paul, T. Acharjee, and S.S. Ramachairy. "Biosensors and their widespread impact on human health ". *Sens. Int.*, **5**:100257, 2024.

[5] A. Pitkänen and J. Engel Jr. "Past and present definitions of epileptogenesis and its biomarkers ". *Neurother.*, **11**(2):231–241, 2014.

[6] Y. Zhou, L. Tao, J. Qiu, J. Xu, X. Yang, Y. Zhang, X. Tian, X. Guan, X. Cen, and Y. Zhao. "Tumor biomarkers for diagnosis, prognosis and targeted therapy ". *Signal Transduct. Target. Ther.*, **9**(1):132, 2024.

[7] J.K. Aronson and R.E. Ferner. "Biomarkers-a general review". *Curr Protoc Pharmacol.*, **76**(1):9–23, 2017.

[8] S. Lv, K. Zhang, Y. Zeng, and D. Tang. "Double photosystems-based 'Z-Scheme'photoelectrochemical sensing mode for ultrasensitive detection of disease biomarker accompanying three-dimensional DNA walker ". *Anal. Chem.*, **90**(11):7086–7093, 2018.

[9] K.K. Jain and K.K. Jain. "The handbook of biomarkers ". *Springer*, 2010.

[10] X. Song, Y. Tao, S. Bian, and M. Sawan. "Optical biosensing of monkeypox virus using novel recombinant silica-binding proteins for site-directed antibody immobilization". *J. Pharm. Anal.*, **14**(10): 100995, 2024.

[11] A. Alnaimi, A. Al-Hamry, Y. Makableh, A. Adiraju, and O. Kanoun. "Gold nanoparticles-MWCNT based aptasensor for early diagnosis of prostate cancer". *Biosensors*, **12**(12):1130, 2022.

[12]

[13] Z. Yu, J. Tang, H. Gong, Y. Gao, Y. Zeng, D. Tang, and X. Liu. "Enzyme-encapsulated protein trap engineered metal–organic framework-derived biomineral probes for non-invasive prostate cancer surveillance ". *Adv. Funct. Mater.*, **33**(26):2301457, 2023.

[14] F. Farshchi and M. Hasanzadeh. "Nanomaterial based aptasensing of prostate specific antigen (PSA): recent progress and challenges in efficient diagnosis of prostate cancer using biomedicine". *Biomed. Pharmacother.*, **132**:110878, 2020.

[15] G. Cai, Z. Yu, R. Ren, and D. Tang. "Exciton–plasmon interaction between AuNPs/graphene nanohybrids and CdS quantum dots/TiO_2 for photoelectrochemical aptasensing of prostate-specific antigen". *ACS sens.*, **3**(3):632–639, 2018.

[16] I.M. Thompson and D.P. Ankerst. "Prostate-specific antigen in the early detection of prostate cancer". *Cmaj.*, **176**(13):1853–1858, 2007.

[17] M. David and S. Leslie. "Prostate-Specific Antigen". *StatPearls*, 2024.

[18] F. Mirzaee Rad, F. Tafvizi, H. Noorbazargan, and A. Iranbakhsh. "Ag-doped ZnO nanoparticles synthesized through green method using Artemisia turcomanica extract induce cytotoxicity and apoptotic activities against AGS cancer cells: an in vitro study". *J. Nanostruct. Chem.*, **14**(6):403–418, 2024.

[19] R. Sundaresan, V. Mariyappan, T.W. Chen, S.M. Chen, M. Akilarasan, X. Liu, and J. Yu. "One-dimensional rare-earth tungstate nanostructure encapsulated reduced graphene oxide electrocatalyst-based electrochemical sensor for the detection of organophosphorus pesticide". *J. Nanostruct. Chem.*, **14**(5):355–368, 2024.

[20] S. Pang, L. Zhao, and Y. An. "Advanced developments in nanotechnology and nanomaterials for the oil and gas industry: a review". *Geoenergy Sci. Eng.*, page 212872, 2024.

[21] N. Al-Harbi and N.K. Abd-Elrahman. "Physical methods for preparation of nanomaterials, their characterization and applications: a review ". *J. Umm Al-Qura Univ. Appl. Sci.*, 2024. DOI: https://doi.org/10.1007/s43994-024-00165-7.

[22] L. Li, T. Wang, Y. Zhong, R. Li, W. Deng, X. Xiao, Y. Xu, J. Zhang, X. Hu, and Y. Wang. "A review of nanomaterials for biosensing applications ". *J. Mater. Chem. B*, **12**(5):1168–1193, 2024.

[23] T. Sathish, N. Ahalya, M. Thirunavukkarasu, T. Senthil, Z. Hussain, M.I.H. Siddiqui, H. Panchal, and K.K. Sadasivuni. "A comprehensive review on the novel approaches using nanomaterials for the remediation of soil and water pollution ". *Alex. Eng. J.*, **36**:373–385, 2024.

[24] G. Paramasivam, V.V. Palem, S. Meenakshy, L.K. Suresh, M. Gangopadhyay, S. Antherjanam, and A.K. Sundramoorthy. "Advances on carbon nanomaterials and their applications in medical diagnosis and drug delivery". *Colloids Surf. B*, page 114032, 2024.

[25] J. Kim, J. Lee, J.M. Lee, A. Facchetti, T.J. Marks, and S.K. Park. "Recent advances in low-dimensional nanomaterials for photodetectors ". *Small Methods*, **8**(2):2300246, 2024.

[26] Y. Wang, R. Zeng, S. Tian, S. Chen, Z. Bi, D. Tang, and D. Knopp. "Bimetallic single-atom nanozyme-based electrochemical-photothermal dual-function portable immunoassay with smartphone imaging". *Anal. Chem.*, **96**(33):13663–13671, 2024.

[27] A.M. Amani, L. Tayebi, E. Vafa, A. Jahanbin, M. Abbasi, A. Vaez, H. Kamyab, and S. Chelliapan. "Innovation applications of MXenes in biomedicine". *Mater. Today Commun.*, page 109929, 2024.

[28] K.R.G. Lim, M. Shekhirev, B.C. Wyatt, B. Anasori, Y. Gogotsi, and Z.W. Seh. "Core–shell nanostructures: perspectives towards drug delivery applications ". *Fundamentals of MXene synthesis, Nat. Synth.*, **1**(8):601–614, 2022.

[29] A.M. Amani, E. Vafa, M. Mirzae, M. Abbasi, A. Vaez, A. Najdian, A. Jahanbin, S.R. Kasaei, S. Mosleh-Shirazi, and H. Kamyab. "Mxenes as a versatile nanoplatform: Synthesis and emerging biomedical applications ". *J. Ind. Eng. Chem.*, 2025. DOI: https://doi.org/10.1016/j.jiec.2025.02.020.

[30] Y. Zeng, Y. Tang, M. Liu, and C. Wu. "Two-dimensional MXene@ ZIF-8 hybrid-derived TiO_2/TiN@ NC heterostructure as an emerging material for electrochemical sensing". *Carbon Lett.*, **34**(7):1887–1898, 2024.

[31] J.C. Lei, X. Zhang, and Z. Zhou. "Recent advances in MXene: Preparation, properties, and applications". *Front. Phys.*, **10**:276–286, 2015.

[32] P. Das and Z.S. Wu. "MXene for energy storage: present status and future perspectives ". *J. Phys. Energy*, **2**(3):032004, 2020.

[33] G. Cai, Z. Yu, P. Tong, and D. Tang. "Ti_3C_2 MXene quantum dot-encapsulated liposomes for photothermal immunoassays using a portable near-infrared imaging camera on a smartphone". *Nanoscale*, **11**(33):15659–15667, 2019.

[34] C. Qiao, H. Wu, X. Xu, Z. Guan, and W. Ou-Yang. "Electrical conductivity enhancement and electronic applications of 2D Ti_3C_2Tx MXene materials ". *Adv. Mater. Interfaces*, **8**(24):2100903, 2021.

[35] Y. Zhou, L. Yin, S. Xiang, S. Yu, H.M. Johnson, S. Wang, J. Yin, J. Zhao, Y. Luo, and P.K. Chu. "Unleashing the potential of MXene-based flexible materials for high-performance energy storage devices". *Adv. Sci.*, **11**(3):2304874, 2024.

[36] S. Zhang, M. Guo, Y. Xia, S. Li, X. Zhi, and X. Wang. "Noncontact monolayered triboelectric nanogenerator based on stretchable MWCNTs/MXene/Ecoflex film for human–machine interface and high-accuracy handwritten recognition ". *J. Chem. Eng.*, **505**:159562, 2025.

[37] A. Sinha, H. Zhao, Y. Huang, X. Lu, J. Chen, and R. Jain. "MXene: An emerging material for sensing and biosensing ". *TrAC, Trends Anal. Chem.*, **105**:424–435, 2018.

[38] H. Liu, C. Duan, C. Yang, W. Shen, F. Wang, and Z. Zhu. "A novel nitrite biosensor based on the direct electrochemistry of hemoglobin immobilized on MXene-Ti_3C_2 ". *Sens. Actuators B*, **218**:60–66, 2015.

[39] A.M. Arjun, M. Shinde, and G. Slaughter. "Application of MXene in the electrochemical detection of neurotransmitters: A Review ". *IEEE Sens. J.*, **23**(15):16456–16466, 2023.

[40] W.X. Huang, Z.P. Li, D.D. Li, Z.H. Hu, C. Wu, K.L. Lv, and Q. Li. "Ti_3C_2 MXene: recent progress in its fundamentals, synthesis, and applications". *Rare Met.*, **41**(10):3268–3300, 2022.

[41] S. Kumar, Y. Lei, N.H. Alshareef, M. Quevedo-Lopez, and K.N. Salama. "Biofunctionalized two-dimensional Ti_3C_2 MXenes for ultrasensitive detection of cancer biomarker ". *Biosens. Bioelectron*, **121**:243–249, 2018.

[42] A.M. Amani, L. Tayebi, E. Vafa, R. Bazargan-Lari, M. Abbasi, A. Vaez, H. Kamyab, S. Rajendran, and M.J. Azizli. "Exploring the revolutionary potential of MXene nanoparticles in breast Cancer therapy: A review of applications and future prospects ". *Int. Immunopharmacol.*, **152**:114411, 2025.

[43] Tayebi L. Vafa E. Jahanbin A. Abbasi M. Vaez A. Kamyab H. Gnanasekaran L. Chelliapan S. Amani, A.M. "MXenes in biosensing: Enhancing sensitivity and flexibility–A review of properties, applications, and future directions". *Sens. Bio-Sens. Res.*, page 100732, 2025.

[44] H.S. Far, M. Najafi, M. Hasanzadeh, and M. Rabbani. "Self-supported 3D-printed lattices containing MXene/Metal–organic framework (MXOF) composite as an efficient adsorbent for wastewater treatment". *ACS Appl. Mater. Interfaces.*, **14**(39):44488–44497, 2022.

[45] M. Nodehi, M. Baghayeri, and H. Veisi. "Preparation of GO/Fe_3O_4@PMDA/AuNPs nanocomposite for simultaneous determination of As^{3+} and Cu^{2+} by stripping voltammetry". *Talanta*, **230**:122288, 2021.

[46] J. Chen, S. Li, Y. Chen, J. Yang, J. Dong, and X. Lu. "l-cysteine-terminated triangular silver nanoplates/MXene nanosheets are used as electrochemical biosensors for efficiently detecting 5-hydroxytryptamine ". *Anal. Chem.*, **93**(49):16655–16663, 2021.

[47] T. He, W. Liu, T. Lv, M. Ma, Z. Liu, A. Vasiliev, and X. Li. "MXene/SnO_2 heterojunction based chemical gas sensors". *Sens. Actuators B*, **329**:129275, 2021.

[48] R. Wang, C. Yao, C. Peng, J. Qiu, Q. Wang, X. Liu, J. Meng, and W. Wang. "Ultra-strong adsorption of organic dyes and antibiotic onto the alk-MXene/ZIF adsorbents with a specific intercalation structure ". *Chem. Eng. J.*, **485**:149916, 2024.

[49] Z. Zhang and H. Karimi-Maleh. "Label-free electrochemical aptasensor based on gold nanoparticles/titanium carbide MXene for lead detection with its reduction peak as index signal ". *Adv. Compos. Hybrid Mat.*, **6**(2):68, 2023.

[50] Z. Zhang and H. Karimi-Maleh. "In situ synthesis of label-free electrochemical aptasensor-based sandwich-like AuNPs/PPy/Ti3C2Tx for ultrasensitive detection of lead ions as hazardous pollutants in environmental fluids". *Chemosphere*, **324**:138302, 2023.

[51] P. Assari, A.A. Rafati, A. Feizollahi, and R. Asadpour Joghani. "An electrochemical immunosensor for the prostate specific antigen based on the use of reduced graphene oxide decorated with gold nanoparticles ". *Microchim. Acta*, **186**:1–9, 2019.

[52] G. Zhang, Z. Liu, L. Fan, and Y. Guo. "Electrochemical prostate specific antigen aptasensor based on hemin functionalized graphene-conjugated palladium nanocomposites ". *Microchim. Acta*, **185**:1–8, 2018.

[53] M. Kukkar, S. Singh, N. Kumar, S.K. Tuteja, K.H. Kim, and A. Deep. "Molybdenum disulfide quantum dot based highly sensitive impedimetric immunoassay for prostate specific antigen". *Microchim. Acta*, **184**:4647–4654, 2017.

[54] X. Hun, Y. Xu, and X. Luo. "Peptide-based biosensor for the prostate-specific antigen using magnetic particle-bound invertase and a personal glucose meter for readout ". *Microchim. Acta*, **182**:1669–1675, 2015.